TWO -DIMENSIONAL COMPUTATION OF SOUND GENERATED BY FLOW AROUND A CIRCULAR CYLINDER

Orselli, R. M., reinaldo.orselli@poli.usp.br
Meneghini, J.R., jmenegh@usp.br
Saltara, F., fsaltara@poli.usp.br
University of Sao Paulo, Escola Politecnica, Mechanical Engineering Department, Sao Paulo-SP, Brazil

Abstract. *The far-field sound generated from low mach number flow around a two-dimensional circular cylinder in the sub-critical regime is computed by the Lighthill acoustic analogy. The time-dependent incompressible flow is predicted using an unsteady Reynolds-averaged Navier-Stokes model. As a benchmark, a flow-field with a Reynolds number of 90,000 is employed. The obtained numerical results such as Strouhal number, fluctuating lift and mean drag are compared with experiments. The computed unsteady pressure fluctuations are used as a sound source for the acoustic solver. The predicted acoustic field is obtained considering on-body and off-body integration surfaces. Comparison between the 2-D numerical results and experiment shows that computed acoustic field overpredict the noise amplitude; however, a good agreement is obtained if an appropriate correlation length is taken into account.*

Keywords: *aeroacoustics, turbulence model, cylinder flow*

1. INTRODUCTION

Due to more restrict environmental noise emission levels, prediction and reduction of aerodynamic noise have been recently a major concern mainly for high speed trains, airplanes and road vehicles. An understanding of the aerodynamic sound sources and its relation to the noise generated is an essential step for reducing or controlling the aeroacoustic noise. One of the main challenging problems in this area is the noise prediction of flows around bluff bodies. The flow around a circular cylinder has been used as a simple and classical representation of bluff bodies flows. Despite its simple geometry, the flow over circular cylinder is a complex phenomenon and very difficult to model numerically. It is characterized by the von Karman vortex street, it is inherently unsteady involving flow separation and laminar-turbulent transition. The von Karman street produces unsteady pressure fluctuations and forces which are the noise sources of the sound generated.

For flows with low Mach number, the coupling between the flow field fluctuations and the acoustic disturbances can be generally neglected, except for some particular cases. Hence, the incompressible unsteady flow can be computed separately, as a noise source, from the acoustical field. The acoustic analogy equations are based on this fundamental assumption, i.e., the unsteady flow generates sound and modifies its propagation, but the sound waves do not affect the flow at all. Thus, the main application of the analogy approach lies at low fluctuating Mach numbers. In this approach, the far-field sound is computed from integral solutions of the wave equation which uses, as a source term, the flow field obtained from the CFD solution.

Following the works of Cox *et al.* (1998) and Gloerfelt *et al.* (2005), in this paper we investigate numerically the flow field and its induced sound generated by a two-dimensional unsteady flow around a circular cylinder with a Reynolds number (based on the cylinder diameter) of 90,000. The Reynolds number is within the range of the subcritical flow regime that is characterized by a laminar boundary layer separation with turbulence transition occurring downstream in the wake. In order to obtain the incompressible flow field, Unsteady Reynolds Average Navier-Stokes (URANS) equations are solved using the software package, FLUENT. Providing the time history of the flow field noise sources, in a post-processing step, the far-field sound is predicted numerically by the integral solution of acoustic analogy equations based on the Ffwocs Williams and Hawkings (FW-H) method presented originally in Ffwocs Williams & Hawking (1969). Despite the fact of the flow being inherently 3-D for Re = 90,000, a two-dimensional numerical simulation can capture the main physical aspects of the flow dominated by an alternate and periodical vortex shedding. Therefore, the present article intends to evaluate the ability of the two-dimensional URANS numerical solutions to predict the unsteady flow over the cylinder and its associated noise generated.

2. GOVERNING EQUATIONS AND NUMERICAL METHODS

In the present work, the far-field sound is predicted by a more general form of the Lighthill acoustic analogy (Lighthill, 1952), developed originally by Ffowcs Williams & Hawkings (1969), which includes the effect of surfaces in arbitrary motion. The near-field source fluctuations of the incompressible flow are first obtained by solving the fluid governing equations whose results are used, as input data, to feed the following acoustical computation. Due to the fact that the acoustic analogy separates the flow field and acoustic computations, acoustic and aerodynamic approaches will be, in general, presented separately.

2.1. Aerodynamic computation methodology

Computational fluid dynamics (CFD) is used to obtain the unsteady flow field. Applying a time averaging (or Reynolds-averaging) to the Navier-Stokes equations (RANS), an additional term, the Reynolds stress tensor, appears which is modeled by making use of the Boussinesq eddy-viscosity approximation. In this assumption the Reynolds stress tensor is computed as product of an eddy viscosity and the main strain rate tensor (Wilcox, 1998). In order to close the system of equations, this eddy turbulent viscosity is related to additional scalar turbulent quantities that are solved by its own transport equations. The turbulence models are usually classified by the number of these added transport scalar equations. It the present paper, the RANS two-equation $k-\omega\ SST$ (*SST* - shear stress transport) model of Menter (1994) is used. It is a hybrid model that makes use of the standard $k-\varepsilon$ model (Launder & Spalding, 1974) equations in the fully turbulent region (far from the walls) and transforms into the $k-\omega$ equations model (Wilcox, 1994) close to wall region. In addition, the eddy viscosity definition is modified to account for the transport of the principal turbulent shear stress. This model gives good results for flows characterized by zero pressure gradient and adverse pressure gradient boundary layers (Versteeg & Malalasekera, 2007) which makes it more appropriate for the problem of the flow over the cylinder. In addition, as a reference, two other classical turbulence models are compared to the $k-\omega\ SST$ model, the $k-\varepsilon$ model and the one-equation Spalart-Allmaras model, *S-A*, (Spallart-Allmaras, 1994), which is a model widely used for airfoil applications in the aerospace and turbomachinery community. In order to use the Reynolds-Averaging of Navier-Stokes equations (RANS) appropriately in unsteady turbulent flows, the time interval should be shorter than the main turbulent structures (for instance, vortex shedding period of the flow over the cylinder) but much higher than the slowest turbulent motion. In this case, only the main turbulent motions may be well resolved by RANS turbulent models. More details of the turbulent motions can be obtained using either Direct or Large-Eddy Simulations.

In order to predict the boundary layer and separation around the cylinder wall, the approach of resolving the near wall-region (viscosity-affected inner region) is used in all employed turbulence models. For the near wall model treatment, the two-layer model originally proposed by Wolfshtein (1969) is applied. In this model, the computational domain is subdivided into a near-wall viscosity-affected region and a fully-turbulent region. In the viscosity-affected region, the turbulent eddy viscosity is related to the turbulent kinetic energy (k) and a near-wall adapted length scale, whose formulation was proposed by Chen & Patel (1988).

A low-Reynolds-number correction to the turbulent viscosity in the standard $k-\omega$ model was proposed by Wilcox (1994). This modification was developed to take into account both the viscous near-wall effects and laminar-turbulent transition at boundary layers flows. This correction was extended to the $k-\omega\ SST$ model which is also used, in the present paper, for solving the fluid flow over the cylinder. This model is referred in the present paper as $k-\omega\ SST\ transition$.

All the numerical simulations were performed using the FLUENT CFD finite-volume code. The numerical discretization scheme employed for the pressure-velocity coupling was the PISO algorithm (originally developed for unsteady compressible flows, Versteeg & Malalasekera, 2007). The upwind second-order spatial differencing method was applied for the convective terms. The solution is time-advanced using an implicit and second-order accurate scheme.

The cylinder diameter (D) is 0.019 m and the freestream Mach Number employed is M = 0.2 corresponding to $Re_D \approx 90{,}000$. A structured mesh with 69,699 cells is employed. The computational domain top and bottom boundaries were both located at 10.5D from the cylinder axis. The inlet and outlet exit were placed, respectively, at 8.5D and 20.5D from the cylinder axis. The cylinder surface is discretized with 240 volume cells. In order to solve the near-wall flow, a spatial mesh resolution of $\Delta y^+ \approx 1$ ($= u_\tau \Delta y / \nu$)) was employed on the cylinder wall. For adequate temporal resolution, each shedding cycle was divided by approximately 234 time steps. Figure 1 shows the computational mesh used in the two-dimensional simulations.

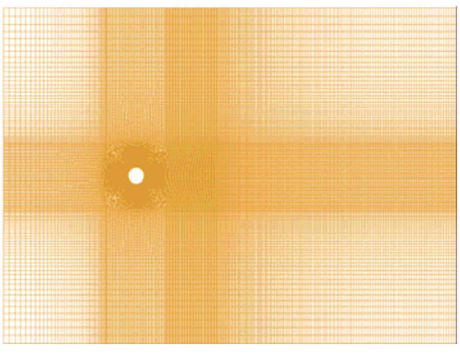

Figure 1. Computational structured mesh for flow around the cylinder, 69,699 volumes cells.

2.2. Acoustic computation methodology

In the acoustic analogy approach, the obtained near-field flow is used as a sound source input into the wave equations to predict the mid-to-far-field noise. It considers that the fluid flow dynamics is completely uncoupled from the acoustic field. The method used here is based on the Ffowcs Williams and Hawkings equations and its integral solution. This model is applicable only to predict the propagation of sound toward the free space (surrounded by a uniform fluid flow at rest). It does not take into account wave reflection or scattering due any additional obstacle (solid surface) between the sound flow-field source and the observer.

The Ffowcs Williams and Hawkings equations can be obtained by just manipulating the continuity and Navier-Stokes equations (more details in Ffwocs Williams & Hawkings, 1969 and Brentner & Farassat, 1998). Essentially, it is an inhomogeneous wave equation:

$$\frac{1}{c_\infty^2}\frac{\partial^2 p'}{\partial t^2}-\nabla^2 p'=\frac{\partial}{\partial t}\left\{\left[\rho_\infty \upsilon_n+\rho(u_n-\upsilon_n)\right]\delta(f)\right\}-\frac{\partial}{\partial x_i}\left\{\left[P_{ij}n_j+\rho u_i(u_n-\upsilon_n)\right]\delta(f)\right\}+\frac{\partial^2}{\partial x_i \partial x_j}\left\{T_{ij}H(f)\right\} \tag{1}$$

where $p' = p - p_\infty$, u_i and υ_i are, respectively, the fluid and surface velocity component in the x_i direction, u_n and υ_n are, respectively, the fluid and surface velocity component normal to the surface ($f = 0$). $\delta(f)$ indicates the Dirac delta function and $H(f)$ correspond to the Heaviside function. A mathematical surface (S) is defined by the function f, $f<0$ represents a region inside S, $f=0$ denotes the surface S and $f>0$ correspond to an unbounded space outside S. n_i is a unit normal vector pointing towards outside S, c_∞ is the freestream speed of sound and T_{ij} is the Lighthill stress tensor, which is given by,

$$\begin{gathered} T_{ij}=\rho u_i u_j+P_{ij}-c_\infty^2(\rho-\rho_\infty)\delta_{ij} \\ where,\ P_{ij}=p\delta_{ij}-\mu\left[\frac{\partial u_i}{\partial x_j}+\frac{\partial u_j}{\partial x_i}-\frac{2}{3}\frac{\partial u_k}{\partial x_k}\delta_{ij}\right] \end{gathered} \tag{2}$$

In Eq. (1) we have a wave equation with three inhomogeneous acoustic source terms on its right hand side known, respectively, as monopole, dipole and quadrupole sources. The monopole source represents the noise generated due mass fluctuation of the fluid by moving surfaces. The dipole source corresponds to noise generated by fluctuating forces on the body surface. The quadrupole source accounts for the noise generation due off body fluctuating shear stresses of the fluid.

The solution of Eq. (1) is obtained by applying the convolution product using the free-space Green function $G(g)=\delta(g)/4\pi r$, where $g=t-\tau-r/c$ with t and τ being, respectively, the observer and source times. The complete solution is expressed by surface and volume integrals. The surface integrals account for the monopole and dipole acoustic sources and partially to the quadrupole sources. The volume integrals represent the quadrupole sources outside the source surface. For flows with low Mach number the volume integrals contribution become small. In addition, if the source surface is placed so that it surrounds all sound sources and its non linear effects, then, it can be shown that all quadrupole noise generated will be represented by the surface integrals. In this case the volume integral should be dropped. The volume integral calculations are very time consuming, thus, in all results, this term is neglected. Dropping the volume integral, the analytical solution of Eq. (1) may be written as (Brentner & Farassat, 1998),

$$\begin{aligned} &p'(\vec{x},t)=p_T'(\vec{x},t)+p_L'(\vec{x},t) \\ &4\pi p_T'(\vec{x},t)=\int_{f=0}\left[\frac{\rho_\infty(\dot{U}_n+U_{\dot{n}})}{r(1-M_r)^2}\right]_{ret}dS+\int_{f=0}\left[\frac{\rho_\infty U_n\left\{r\dot{M}_r+c_\infty(M_r-M^2)\right\}}{r^2(1-M_r)^3}\right]_{ret}dS \\ &4\pi p_L'(\vec{x},t)=\frac{1}{c_\infty}\int_{f=0}\left[\frac{\dot{L}_r}{r(1-M_r)^2}\right]_{ret}dS+\int_{f=0}\left[\frac{L_r-L_M}{r^2(1-M_r)^2}\right]_{ret}dS+\frac{1}{c_\infty}\int_{f=0}\left[\frac{L_r\left\{r\dot{M}_r+c_\infty(M_r-M^2)\right\}}{r^2(1-M_r)^3}\right]_{ret}dS \end{aligned} \tag{3}$$

In Eq. (3), new variables $U_i=[\upsilon_i+\rho/\rho_\infty(u_i-\upsilon_i)]$ and $L_i=P_{ij}\hat{n}_j+\rho u_i(u_n-\upsilon_n)$ are introduced, where $U_n=\vec{U}\cdot\vec{n}=U_i n_i$ and $L_r=\vec{L}\cdot\hat{\vec{r}}=L_i r_i$, $\vec{n}$ and $\vec{r}$ correspond to unit vectors, respectively, in the surface normal direction and in the radiation direction, respectively. The square brackets with the subscript ret denote that the integrands are computed at the retarded time when the sound was emitted, $\tau = t - r / c_\infty$, where t is the time at the observer and r is the distance between the sound source and the observer. The dot over the variable represents source-time differentiation of the variable (i.e., $U_{\dot{n}}$ is $U_n \partial n_i / \partial \tau$). Also, $\vec{M}$ is a local Mach number vector with components M_i, where $M_r = \vec{M} \cdot \hat{\vec{r}} = M_i r_i$ and $L_M = L_i M_i$.

When the source or integration surface is placed on the body (impermeable wall), the terms, in Eq. (3), $p_T^{'}(\vec{x},t)$ and $p_L^{'}(\vec{x},t)$ are known as thickness and loading noise, respectively, related to its physical meanings. In this formulation, the source surface ($f = 0$) does not have to be placed on body surfaces or walls. The integration surface can be located in the interior flow (off body surface). In this case the surface is permeable and the surface integrals of Eq. (3) take into account the contributions of the quadrupole noise sources inside the region enclosed by the source surface. It should be noted that within the permeable surface, the grid resolution needs to be fine enough to resolve all significant unsteady flow structures. This specific approach is known as porous FW-H formulation. In the present work, all acoustic results were obtained utilizing the software package, FLUENT.

3. AERODYNAMIC RESULTS

In order to obtain the acoustic far-field, the near-field unsteady flow results are used as an input data to the wave equations, Eq. (1). Thus, the noise prediction depends directly on the accuracy of the CFD results. In this paper, the two-dimensional unsteady versions of the turbulence models $k-\omega$ *SST transition*, $k-\omega$ *SST*, S-A and $k-\varepsilon$ are used for obtaining the time-history of the near-field flow over a circular cylinder at $\mathrm{Re}_D = 90{,}000$. In all simulations, it was investigated the mesh refinement effects on the numerical results, no more refinement was considered to be necessary for a mesh with 69,669 volumes, Fig. 1.

The accuracy of the numerical simulations is generally evaluated by comparing it with available experimental results. For bluff bodies, mean flow quantities such as mean drag coefficient ($\bar{C}_d$) and angle of flow separation (θ_s) and, also, fluctuating quantities such as shedding frequency ($S_t = fU_\infty / D_{cyl}$) and r.m.s. of drag and lift coefficient (respectively, $C_l^{'}$ and $C_d^{'}$) are commonly used as benchmark parameters for evaluating the quality of the CFD results in comparison with its corresponding available experimental data. In Tab. 1, it is shown the obtained results of the two-dimensional numerical simulations using the indicated U-RANS models with which can be compared to the experimental data.

Table 1. Experimental data and obtained numerical results (69,699 cells volumes grid) of S_t, $C_l^{'}$, , $\bar{C}_d$, $C_d^{'}$ and θ_s.

	S_t	$C_l^{'}$	$\bar{C}_d$	$C_d^{'}$	θ_s
Experimental data	0.180-0.191 Norberg (2003)	0.45-0.60 Norberg (2003)	1.0-1.4 Cantwell & Coles (1983)	0.18 West (1993)	80º Achenbach (1968)
$k-\omega$ *SST transition*	*0.235*	*0.823*	*1.09*	*0.062*	*88º*
$k-\omega$ *SST*	*0.247*	*0.762*	*0.944*	*0.061*	*99º*
S-A	*0.242*	*0.165*	*0.625*	*0.0031*	*96º*
$k-\varepsilon$	*0.282*	*0.090*	*0.479*	*0.0013*	*109º*

In Tab. 1, it can be noted that each turbulent model produced quite different results for all flow quantities. The highest values of r.m.s of C_l, mean and r.m.s. of C_d were obtained by the $k-\omega$ *SST transition* model. The results shows that the values of $C_l^{'}$ and $\bar{C}_d$ are very sensitive to the choice of the turbulent model. In comparison with the experimental data, all turbulence models predicted a slightly higher shedding frequency. The overprediction of the shedding frequency from two-dimensional computation is an expected CFD result. As argued by Casalino, 2003, in the 2-D simulation the mean Reynolds stresses are higher (in comparison to 3-D flows) corresponding to shorter mean recirculating regions, as a consequence, the recirculating regions are slightly closer resulting in a higher Strouhal frequency. It can be observed a direct relation of the lift and drag fluctuations and mean drag to the point of the flow separation. The farther the point of separation occurs, the lower are the fluctuating forces and the mean drag. Thus, the ability of the turbulence model to predict separation determines much of the flow behavior around the cylinder. Comparing the $k-\omega$ *SST transition* and $k-\omega$ *SST*, which differs only from their near-wall approach, it can be noted the superior performance of the low- Reynolds near-wall approach of Wilcox (1994) dealing with separating flows. The fact that this near wall approach takes into account local laminar-turbulent transition may have contributed to emulate the flow separation physics. Therefore, the most accurate turbulent model is the $k-\omega$ *SST transition*, despite its higher

$C_l^{'}$ values which is mostly related to the fact that the 2-D simulation considers the vortex shedding fully correlated along the cylinder span.

The time history of the aerodynamic forces (lift and drag) acting on the cylinder is presented in Fig. 2a. It can be observed that the 2-D U-RANS model predicts an almost perfectly periodic flow which indicates the presence of a fully spanwise correlated main vortex shedding. The Strouhal number corresponding to the main shedding frequency can be obtained by spectral analysis of the lift fluctuations shown by the maximum peak in Fig. 2b. Moreover, in Fig. 2b, it is noted peaks at odd harmonics frequencies (f_0 , $3f_0$, …) for the unsteady lift spectra and peaks at even harmonics ($2f_0$, $3f_0$, …) for the unsteady drag spectra. Thus, the aerodynamic forces acting in the streamwise direction fluctuates at twice the frequency of those in the vertical direction, but the amplitude of the vertical fluctuating forces are much more significant then the forces in the streamwise direction.

(a) 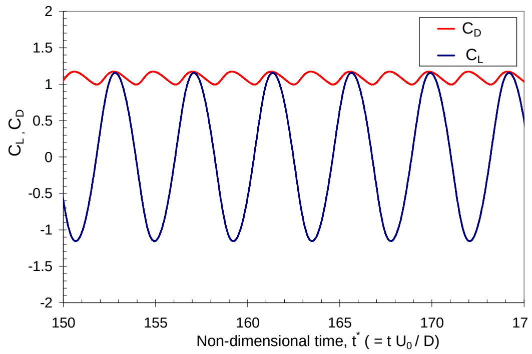

(b) 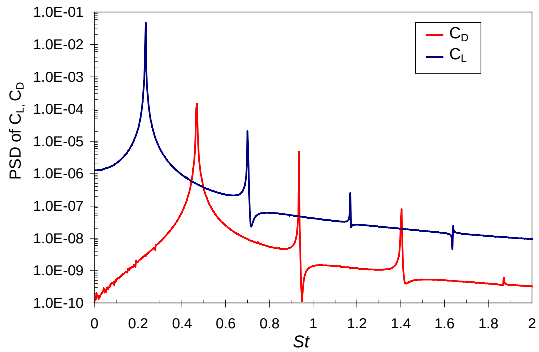

Figure 2. Aerodynamic forces on the cylinder: (a) C_l and C_d time variations; (b) C_l and C_d power spectral density.

4. ACOUSTIC RESULTS

In this section, it is presented the predicted far-field sound computed by the wave equation (Eq. (1)) using the CFD unsteady calculations as input data. In all acoustic computations, the flow field is obtained by the $k-\omega$ *SST transition* model. The experimental data of Revell *et al.* (1977) was chosen to be compared to the acoustic numerical results. The experiments consisted of a flow over a circular cylinder conducted in a freejet anechoic wind tunnel. In this paper, it was used the experimental acoustic data obtained with a microphone posited 90º from the cylinder stagnation point and located at 128 cylinder diameters away from the cylinder axis. The cylinder diameter was 0.019 m with a span length of $25.3D$. The tests were performed with a flow of Mach number 0.2 and a Reynolds number based on the cylinder diameter of 89,000.

In the far field noise computations at the observer ($128D$ way from the cylinder), it was stored 8192 acoustic pressures covering approximately 70 vortex shedding cycles, which permitted a greater spectrum resolution.

The acoustic results are presented in terms of sound pressure level in the decibel scale (dB). The sound pressure level (SPL) is defined as,

$$SPL = 20\log(P_e / P_{ref}) \tag{4}$$

where P_e is the effective sound pressure which corresponds to its root mean square and P_{ref} denotes a reference pressure, it is used a value of $20\,\mu Pa$ in air. For the sound spectrum, SPL values are plotted against its corresponding frequency. In this case, the SPL is computed considering the effective pressure (P_e) as the amplitude spectrum of the fluctuating acoustic pressure data. Using the acoustic spectrum results, an overall sound level (OASPL) can be obtained by adding all noise amplitudes of the spectrum, the $OASPL$ can be obtained applying the following expression:

$$OASPL = 20\log\sqrt{\sum_i (10^{SPL_i/20})^2} \tag{5}$$

Due to the low Mach number ($M = 0.2$), the contribution of quadrupole sources is not very significant, thus most of the sound is generated on wall surfaces (dipole and monopole sources). Therefore, the acoustic spectrum was here computed considering all noise sources being generated on the cylinder wall surface.

The acoustic experimental data were obtained in a $25.3D$ cylinder span length, however the fluctuating near-field flow were calculated in a two-dimensional computational domain. Thus, in order to compute the acoustic field, information of the flow in the spanwise direction is needed. In the case of a two-dimensional CFD input, the noise is computed assuming that the vortex shedding is perfectly correlated over the entire span of the cylinder. For $\mathrm{Re}_D = 90{,}000$, the fluid flow is not completely correlated in the spanwise direction (three-dimensional flow), which may affected the prediction of overall noise. A way of evaluating the degree of the flow spanwise correlation is by calculating a spanwise correlation length of the lift forces as shown in Norberg (2003). In the reference, it is presented the spanwise correlation length of the cylinder flow in function of the Reynolds number. In the case of a $\mathrm{Re}_D = 90{,}000$, Norberg (2003) provides an average correlation length of 3.16 D. In order to assess the effect of the correlation length on the overall noise prediction, five correlation lengths were tested. Fig. 3 shows the acoustic spectrum obtained applying the different correlation lengths, the flow results were computed with the 2-D $k-\omega$ *SST transion* model. Also, in Tab. 2, it is presented the overall sound noise level (*OASPL*) calculated for the same five different correlation lengths. The results clearly demonstrate that the correlation length affects significantly the noise prediction. It is observed that using the same correlation length of the experiments (25.3 D), the predicted sound level is much overpredicted. In addition, using the flow correlation length of 3.16 D, the predicted overall noise was 3 dB lower than results of Revell *et al.* (1977). Table 1 and Fig. 3 shows that the most accurate noise prediction was obtained with a correlation length of 5.0 D, which can be interpreted as a representative correlation length that matches the computed sound levels with the ones obtained experimentally with a 25.3 D cylinder length.

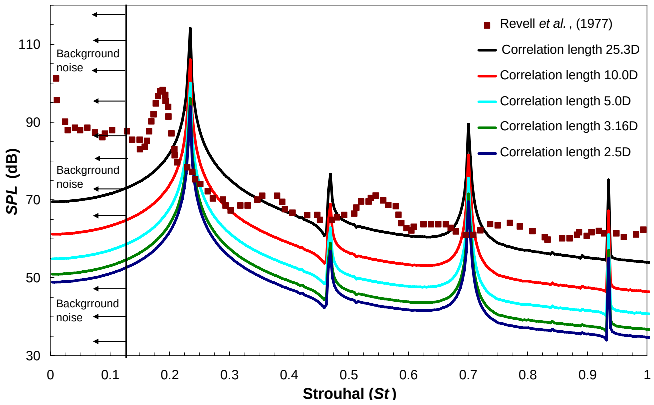

Figure 3. Comparison of sound pressure level spectra for different correlation lengths with the experimental results of Revell *et al.* (1977). Microphone located 128 D away from the cylinder, positioned 90º from the stagnation point.

Table 2. *OASPL* results obtained with different correlation lengths. Revell *et al.* (1977) measured a *OASPL* of 100 dB.

	Correlation length					Measurements (Revell *et al.*, 1977)
	2.5 D	3.16 D	5.0 D	10.0 D	25.3 D	
OASPL (dB)	*94.9*	*96.9*	*100.9*	*106.9*	*114.9*	100.0

In order to investigate the effect of the integration surface location on the noise prediction, a circle off-body surface of 2.0 D diameter was chosen as displayed in Fig. 4. Applying the off body surface, part of the quadrupole sources will be considered in the sound computation. In this case, the contribution of the quadrupole sources will depend on the size of the integration surface and on the grid refinement inside the region enclosed by the permeable surface. Thus, a finer mesh with 152,285 volume cells was built, with the purpose of evaluating the influence of grid resolution inside the integration region. Table 3 presents the obtained *OASPL* noise levels applying both on body and off body surface. The results show that the choice of an off body has little influence on the computed overall noise, which confirms that, due the low Mach number of the flow, the contribution of the quadrupole noise is small or may be neglected. In addition, comparing both mesh grids, it is noted that the contribution of quadrupole noise souces increases four times with the finer mesh, which is probably due a greater numerical diffusion of the coarser mesh.

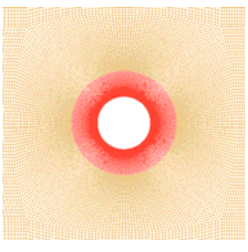

Figure 4. Mesh representation showing the off body integration surface. Meshgrid with 69,699 cell volumes.

Table 3. $OASPL$ results with on body and off body integration surfaces. Cylinder correlation length of 5.0 D .

	Integration surface		
Grid cell volumes	on cylinder	off cylinder (2.0 D)	Difference
69,699	*100.91* dB	*100.96* dB	0.053 dB
152,285	*101.12* dB	*101.31* dB	0.197 dB

A more complete representation of the acoustic field can be obtained by plotting its field directivity, which were computed for an observer located 128 D away from a 5.0 D cylinder length. In Fig. 5, it is presented the overall sound pressure level ($OASPL$), and the sound pressure levels in the fundamental and first harmonic frequencies, which were computed considering an on-body surface. In the figure, the 90º location is at the top and the axes units are in dB. Observing the noise levels directivities, the plotted $OASPL$ and fundamental frequency shapes are nearly symmetrical whereas for the first harmonic, right side noise levels are more pronounced, which means that flow fluctuations on the cylinder wake side affects more the first harmonic sound levels in the downstream direction. In addition, analyzing the directivity shapes of the $OASPL$, fundamental frequency and first harmonic, it can be noted that most of the overall sound level generated at top or botton (Fig. 5a) is due its corresponding noise level in the fundamental frequency (Fig. 5b). In addition, at left and right of the $OASPL$ directivity (Fig. 5a), it is the corresponding noise levels in the first harmonic frequency (Fig. 5c) that dominate the overall radiated noise.

In order to evaluate the relation between the pressure fluctuations on the cylinder wall (the sound sources), and the noise radiated to the observer, directivities of the wall pressure fluctuation levels are plotted in Fig. 6. Figure 6a presents the directivity of the effective values (root mean square) of the fluctuating wall pressures in decibel scale, which, in fact, correspond to an overall wall pressure noise level. In addition, Figures 6b and 6c show the directivity of the wall pressure fluctuation levels in the fundamental and first harmonic frequencies, respectively, divided by its components in the lift (C_l) and drag (C_d) directions. Comparing the corresponding directivities of the pressure levels displayed in Fig. 6 and Fig. 5, a similar shape can be clearly observed, which indicates a tight relation between the fluctuating forces acting on the cylinder ($C_l^{'}$ and $C_d^{'}$) and the propagating sound at the observer.

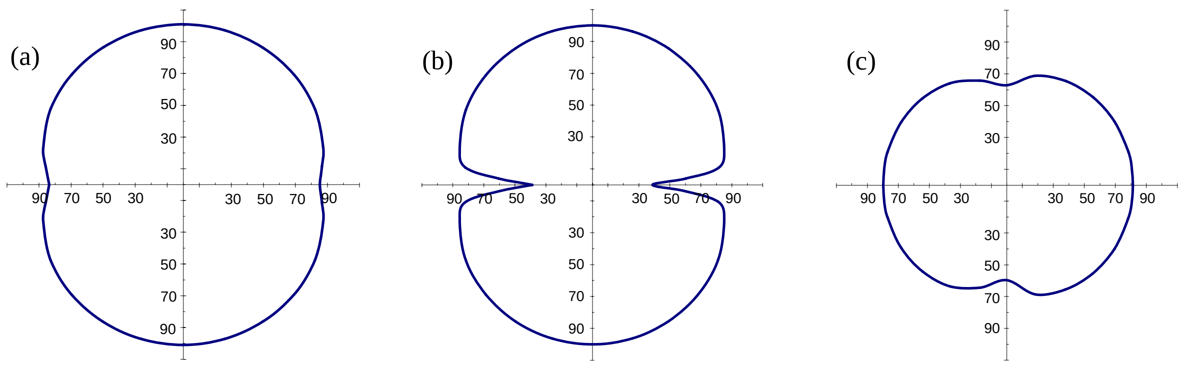

Figure 5. Predicted noise levels directivity patterns: (a) OASPL; (b) fundamental frequency; (c) first harmonic. A meshgrid with 69,699 cell volumes were used for obtaining the displayed results. Observer located 128 D away from the cylinder axis. Axes units are in decibels.

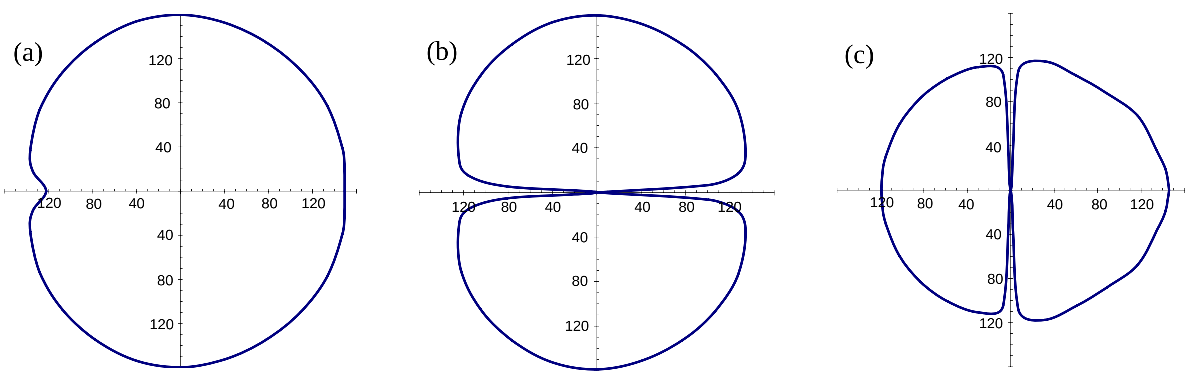

Figure 6. Directivity pattern of the pressure fluctuation levels on the cylinder wall: (a) Overall pressure level (r.m.s values); (b) Fundamental frequency pressure level in the C_l direction; (c) Fisrt harmonic pressure level in the C_d direction. Axes units are in decibels.

5. CONCLUDING REMARKS

The acoustic field is obtained by the integral solution of a wave equation that uses the unsteady CFD results as an input data (Lighthill acoustic analogy). As a first approach, we investigated the ability of two-dimensional CFD results to predict the flow field and the associated radiated noise. Some two-dimensional U-RANS turbulence models were tested for solving a three-dimensional flow over a circular cylinder with $\mathrm{Re}_D = 90,000$. It was concluded that the most accurate turbulence model was the $k-\omega$ *SST transition* model, however the r.m.s values of C_l and S_t were overpredicted, which is probably due the 2-D computations that considers the flow fully correlated over the span direction. The acoustic results showed that the sound prediction is highly dependent on the accuracy of the CFD results. When using 2-D flow field results for sound computation, the flow is assumed completely correlated in the spanwise direction, as a consequence the sound levels are much overpredicted. However, these simulations can predict comparable peak noise amplitudes with experiments if an appropriate correlation length is used. Finally, no significant difference in the predicted overall noise was found when choosing an off body integration surface meaning that, in this case, the contribution of quadrupole noise sources can be neglected.

6. ACKNOWLEDGEMENTS

The authors are thankful to CAPES Brazil, for their financial support during the course of this research.

7. REFERENCES

Achenbach, E., 1968, “Distribution of Local Pressure and Skin Friction in Cross Flow Around a Circular Cylinder up to Re = $5\mathrm{x}10^6$”, J. Fluid Mech., Vol. 34, pp. 625-639.

Brentner, K. S. and Farassat, F., 1998, “Analytical Comparison of the Acoustic Analogy and Kirchhoff Formulations for Moving Surfaces”, AIAA Jornal, Vol. 36, No. 8, pp..1379-1386.

Cantwell, B. and Coles, D., 1983, “An Experimental Study of Entrainment and Transport in the Turbulent Near Wake of Circular Cylinder”, J. Fluid Mech., Vol. 136, No. , pp. 321-374.

Casalino, D. and Jacob, M., 2003, “Prediction of Aerodynamic Sound from Circular Rods via Spanwise Statiscal Modelling”, J. Sound and Vibration, Vol. 262, No. 4, pp. 815-844.

Chen, H.C. and Patel, V.C., 1988, “Near-Wall Turbulence Models for Complex Flows Including Separation”, AIAA Journal, Vol. 26, No. 6, pp.641-648.

Cox, J. S, Brentner, K.S. and Rumsey, L., 1998, “Computation of Vortex Shedding and Radiated Sound for a Circular Cylinder: Subcritical to Transcritical Reynolds Numbers”, Theoretical and Computational Fluid Dynamics, Vol. 12, No. 4, pp. 233-253.

Ffowcs Williams, J. E. and Hawkings, D. L., 1969, “Sound Generated by Turbulence and Surfaces in Arbritary Motion”, Philosophical Transactions of the Royal Society, Vol. A264, No. 1151, pp. 321-342.

Gloerfelt, X., Bailly, C. and Juvé, D., 2003, “Direct Computation of the Noise Radiated by a Subsonic Cavity Flow and Application of Integral Methods”, J. Sound and Vibration, Vol. 266, pp. 119-146.

Lighthill, M. J., 1952, “On Sound Generated Aerodynamically, I: General Theory”, Proc. Royal Society, Vol. A221, pp. 564-587.

Launder, B.E. and Spalding, D.B., 1974, “The Numerical Computation of Turbulent Flows”, Computer Methods in Applied Mechanics and Engineering, Vol. 3, pp.269-289.

Menter, F. R., 1994, “Two-Equation Eddy-Viscosity Turbulence Models for Engineering Applications”, AIAA Journal, Vol. 32, No. 8, pp. 1598-1605.

Norberg, C., 2002, Fluctuating Lift on a Circular Cylinder: Review and New Measurements, J. Fluids and Structures, Vol. 17, No. 1, pp.57-96.

Revell, J. D., Prydz, R. A. and Hays, A.P., 1977, “Experimental Study of Airframe Noise vc. Drag Relationship for Circular Cylinders”, Lockheed Report 28074, Final Report NASA Contract NAS1-14403.

Spalart, P.R. and Allmaras, S.R., 1994, “ A one-equation turbulence model for Aerodynamic Flows. La Recherche Aérospatiale, Vol. 1, pp. 5-21.

Versteeg, H. K., Malalasekera, W., 2007, “An Introduction to Computational Fluid Dynamics”, 2nd ed., Pearson Eductated Lt., Harlow, England.

West, G.S. and Apelt, C. J., 1993, “Measurements of Fluctuating Pressures and Forces on a Circular Cylinder in the Reynolds Number Range 10^4 to $2.5\mathrm{x}10^5$”, J. Fluids and Structures, Vol. 7, No. 3, pp. 227-244.

Wilcox, D. C., 1998, “Turbulence Modeling for CFD”, DCW Industries Inc., La Canada, Ca..

Wolfshtein, M., 1969, “The Velocity and Temperature Distribution in One-Dimension Flow with Turbulence Augmentation and Pressure Gradient”, Int. J. of Heat and Mass Transfer, Vol. 12, No. 3, pp-301-318.

8. RESPONSIBILITY NOTICE

The authors are the only responsible for the printed material included in this paper.